Research Square

Preprints are preliminary reports that have not undergone peer review.
They should not be considered conclusive, used to inform clinical practice,
or referenced by the media as validated information.

Self-Assembled Tetrahedral Framework Nucleic Acid Mediated Tumor-Associated Macrophages Reprogramming and Enhancing Cancer Immunotherapy

husun qian
Chongqing Medical University
Yixin Fu
Chongqing Medical University
Minkang Guo
Chongqing Medical University
Wu Yang
Chongqing Medical University
Dian Zhang
Chongqing Medical University
Ting Zhou
Chongqing Medical University
Wenli Fang
Chongqing Medical University
Mengli Yao
Chongqing Medical University
He Shi
Chongqing Medical University
Chai Chengsen
Chongqing Medical University
Wei Cheng
Chongqing Medical University
Shijia Ding
Chongqing Medical University
tingmei chen (tingmeichen@cqmu.edu.cn)
Chongqing Medical University https://orcid.org/0000-0002-8767-0757

Research

Keywords: TAMs, CpG ODNs, PI3Kγ siRNA, tFNA, cancer treatment

Posted Date: April 1st, 2021

DOI: https://doi.org/10.21203/rs.3.rs-373672/v1

License: This work is licensed under a Creative Commons Attribution 4.0 International License.
Read Full License

Abstract

There is increasing interest in depleting or repolarizing tumor-associated macrophages (TAMs) to generate a pro-inflammatory effect. However, TAMs usually display an immunosuppressive M2-like phenotype in tumor microenvironment. Apparently, developing a macrophage targeting delivery system with immunomodulatory agents is urgent. In the study, an efficient siRNAs and CpG ODNs delivery system (CpG-siRNA-tFNA) was prepared with nucleic acid stepwise self-assembled. The tFNA composed of CpG ODNs and siRNAs showed a higher stability and an enhanced cellular uptake efficiency. Moreover, the CpG-siRNA-tFNA effectively reprogrammed TAMs toward M1 phenotype polarization with increased pro-inflammatory cytokines secretion and NF-κB signal pathways activation, which triggers dramatical antitumor immune responses. Hence, we have developed an efficient and reliable TAM-targeted therapeutic with immunomodulatory agents for for clinical applications.

Introduction

Tumor-associated macrophages (TAMs) are mainly derived from monocytes in the blood circulation and tissue-resident macrophages, which constitute up to 50% of cell populations in tumor mass [1, 2]. As an important component of tumor microenvironment (TME), TAMs play a key role in tumor growth, invasion and metastasis [3, 4]. According to different activation manners, TAMs are divided into classically activated M1 phenotype and alternatively activated M2 phenotype [5]. Most studies have shown that M1 macrophages initiate pro-inflammatory cytokine production, activate immune response and tumoricidal activity [6, 7]. Conversely, M2 macrophages secrete anti-inflammatory cytokine, suppress adaptive immunity and facilitate tumor growth and progression [8, 9]. Of note, TAMs usually display an immunosuppressive M2-like phenotype under the influence of the TME, such as hypoxia and acidity pH [10-12]. In addition, clinical studies have further shown that the presence of TAMs in TME are related to a poor prognosis in a variety of human cancers [13-15]. Thus, it is a potential therapeutic strategy to reprogramme TAMs toward antitumoral M1 macrophages polarization for tumor eradication.

In recent years, TAMs have emerged as an attractive potential therapeutic target for cancer immunotherapy. So far, a variety of immune modulators mediated TAMs-M1 reprogramming have been applied to restore the antitumoral immunity, such as microRNA, cytosine-guanosine oligodeoxynucleotides (CpG ODNs), small interfering RNA (siRNA), antisense oligodeoxynucleotide (ASO), and small molecule inhibitor [16-21]. Among these, siRNA is a powerful molecular tool to knock down specific gene expression in the field of gene therapy. It interferes with the expression of specific genes with complementary nucleotide sequences by degrading mRNA after transcription within the RNA interference pathway [22-24]. However, there are some drawbacks to hinder this free form of siRNA therapeutic efficiency, including low efficiency of cellular uptake, poor stability, and short period of action [25, 26]. Apparently, developing a delivery system that can effectively overcome these challenges and specifically deliver siRNA to TAMs is urgent.

DNA framework nucleic acid (FNA) is an emerging field of DNA-based nanotechnology with controllable size and shape, including DNA origami, tetrahedra, triangle, Y-shaped and so on [27, 28]. Moreover, many studies reported that self-assembled DNA FNA can efficiently deliver various immune modulators into cells due to its inherent biocompatibility, high biosecurity and low cost. For example, Zhang *et al*. developed a DNA tetrahedron-based nanogels based on a crosslinking strategy for intracellular EGFR siRNA delivery, which can efficiently enter the cells and downregulation of the EGFR gene expression [29]. Ding *et al*. fabricated a versatile triangular DNA origami to co-deliver siRNA and chemo-drugs into target cells for enhanced synergistic antitumor effect [30]. Shi *et al*. reported a novel spherical nucleic acid conjugate with superior biocompatibility for siRNA delivery, which showed potent gene knockdown at both mRNA and protein levels [31]. Sleiman *et al*. designed a flexible DNA “nanosuitcase” for siRNA-encapsulating and release it in live cells on demand [32]. These self-assembled DNA FNA could effectively deliver additional therapeutic components into cells with improved dispersity and stability, and thus enhance the therapeutic efficacy.

Here we explored a facile strategy of linking siRNAs and CpG ODNs to a tetrahedral framework nucleic acid (tFNA) to combine targeted delivery to TAMs cells. As shown in Scheme 1A, six DNA strands with complementary overhangs at the 3' ends can self-assemble into a tFNA, which is different from traditional DNA tetrahedral based four DNA strands assembly. We designed the tFNA contains a nick in the middle position of each edge. The overhang at this nick is complementary to the siRNA (AS)-overhang strands. Moreover, the siRNA (SS)-CpG strands also integrated to the tFNA by complementary base pairing of sense strand and antisense strand of the siRNA. Specifically, the tFNA with controllable loading density can simultaneously deliver siRNAs and CpG ODNs into cells. As is well known, CpG ODNs could be efficiently internalized by macrophages with toll-like receptor 9 (TLR9) dependent activation [33]. The binding of TLR9 and CpG ODNs can trigger innate and adaptive immune responses [34]. As an immunostimulatory TLR9 agonist, CpG ODNs are already in preclinical studies for melanoma [35].

Meanwhile, it is reported that PI3Kγ acts as a molecular switch turning on immunosuppression while shutting down immune-stimulatory activities in TAMs [36]. In particular, most studies have shown that PI3Kγ inhibition facilitate M2-like TAMs toward M1 phenotype polarization [37, 38]. Additionally, PI3Kγ also restrains toll-like receptors (TLRs) mediated inflammation and signaling pathway activation [39, 40], we hypothesis that simultaneously inhibition PI3Kγ and activating TLRs could effectively reprogram TAMs toward a more proinflammatory phenotype and inhibit tumor progression. As shown in Scheme 1B, the binding of CpG ODNs and TLR9 facilitated the uptake of the siRNA component into the cytosol for efficient gene silencing. As such, PI3Kγ inhibition effectively enhanced CpG ODNs activation function for the NF-kB signaling pathway. At last, the combination of CpG ODNs immunostimulation and PI3Kγ expression downregulation would effectively reprogramme TAMs toward M1 phenotype polarization and exhibition a potent anticancer efficacy.

Results And Discussion

Preparation and characterization of CpG-siRNA-tFNA

CpG-siRNA-tFNA could be readily prepared using designed strand (Table S1), and the self-assembled process was presented in Scheme 1A. In order to demonstrate stepwise assembly procedure, we separately constructed tFNA, CpG-tFNA and CpG-siRNA-tFNA. The successful preparation of nucleic acid nanostructures was confirmed by gel electrophoresis. As showed in Figure 1A, a distinct band shift was observed along with different strands introduced, indicating tFNA assembly nanostructure formation. For different valence numbers CpG-tFNA nanostructures formation, CpG-overhang strands were added together in different proportions. The gel electrophoresis analysis results were showed in Figure 1B. The band mobility slightly decreased with the increasing of CpG-overhang strand number, which was attributed to slight difference in each nanostructure molecular weight. Similarly, different valence numbers CpG-siRNA-tFNA were constructed and analyzed by gel electrophoresis. As showed in Figure 1C, the band mild movement was observed with the increasing of siRNA (SS)-CpG strand and siRNA (AS)-overhang strand number. The results suggested these functional nucleic acid nanostructures have been successfully synthesized. Moreover, that showed CpG and siRNA could be modified to tFNA with controllable density. Also, The CpG-siRNA-tFNA structure was imaged by atomic force microscopy (AFM), the results were were shown in Figure S1.

Since DNA tFNA was reported to effectively resist nuclease degradation [41], we investigated the stability of tFNA in 10% non-inactivated fetal bovine serum. We compared the stability of dsDNA and tFNA at 37°C for different time periods. As shown in Figure 1D, the band of dsDNA almost disappeared with 3 h incubation. On the contrary, the band of tFNA remained nearly unchanged after 3 h incubation. However, we observed that the band of tFNA gradually moved down and diffused with incubation time extended, especially after 24 h. The phenomenon reflected the tFNA nanostructure suffered partial degradation. Nevertheless, there still was strong band of tFNA after 24 h incubation. Therefore, the tFNA could resist nuclease degradation and possessed a higher stability than dsDNA in fetal bovine serum.

Cell uptake and cytotoxicity of DNA tetrahedral nanostructures

Cellular uptake efficiency of DNA tetrahedral nanostructures was investigated with a fluorescently labeled CpG strand. Confocal imaging showed that CpG-tFNA group presented intense FAM fluorescence in the cytoplasm (Figure 2A). In contrast, the CpG control group showed negligible fluorescence. The phenomenon was consistent with fluorescence microscope imaging (Figure S2). The results suggested that tFNA nanostructure was more readily taken up by cells, which might be also related to the higher stability of tFNA and the ability of tFNA in driving the nanostructures into cells.

The viability of RAW264.7 cells exposed to different concentrations of CpG-tFNA and CpG-siRNA-tFNA were evaluated with a standard CCK-8 assay. As shown in Figure 2B, there were no measurable effect on cells metabolic activity and CpG-tFNA and CpG-siRNA-tFNA even both stimulated the growth of cells. Moreover, CpG-tFNA and CpG-siRNA-tFNA both exhibited more significant stimulation efficiency along with increasing nanostructures concentration, which attributed to the immunostimulatory activity of CpG motifs.

Immunostimulation effects of CpG-siRNA-tFNA

To evaluate the immunostimulatory activity of CpG-siRNA-tFNA, the secretion levels of proinflammatory cytokines (TNF-α, IL-6, and IL-12) in RAW264.7 cells were measured by ELISA. As demonstrated in Figure 3, CpG-tFNA showed significantly increased immunostimulatory activity for the proinflammatory cytokines secretion compared with free CpG ODNs. The results were primarily attributed to the greatly enhanced stability and cellular uptake efficiency of CpG-tFNA. Moreover, the induction of proinflammatory cytokines level was further improved with increasing the number of CpG motifs per tFNA nanostructure. More importantly, CpG-siRNA-tFNA showed much stronger immunostimulatory capability, which induced dramatically higher amounts of the cytokines secretion. This phenomenon indicated the proinflammatory cytokines secretion was synergistically triggered by both CpG ODNs stimulation and PI3Kγ inhibition. Silencing of PI3Kγ enhanced CpG ODNs mediated immunostimulatory activity in RAW264.7 cells. These results also show the tFNA nanostructures possess special superiority that can simultaneously carry siRNAs and CpG ODNs with high loading density. As such, qPCR results of the proinflammatory cytokine levels were consistent with the ELISA (Figure S3).

Macrophages polarization by immunostimulatory CpG-siRNA-tFNA

To validate the macrophages polarization markers, RAW264.7 were treated with LPS and IL-4 for 24h, respectively. The western blot results (Figure S4B) confirmed the expression of M1 marker (iNOS) and M2 marker (Arg-1). In addition, we observed the morphological changes in different types polarization of macrophages (Figure S4A).

As is well known, the enhanced secretion of proinflammatory cytokines is a major characteristic of M1 phenotype macrophages. And NF-κB are the major signal pathways participating in the expression of a variety of cytokines after the stimulation of CpG-siRNA-tFNA. Therefore, we investigated the macrophages phenotype transformation and NF-κB signal pathways activation. As showed in Figure 4A, CpG-siRNA-tFNA induced iNOS expression and stimulated NF-κB p65 subunit phosphorylation in RAW264.7 cells. More importantly, PI3Kγ inhibition increased CpG-inducible iNOS expression and CpG-stimulated phosphorylated p65 expression levels.

Subsequently, we investigated whether PI3Kγ expression downregulation promoted M2 macrophages toward M1 phenotype polarization. Macrophages were first induced toward M2 phenotype polarization upon stimulation with IL4. Consistent with previous studies, IL4 induced a remarkably Arginase 1 expression (Figure 4B). Whereas, PI3Kγ knockdown evidently inhibited Arg1 expression and enhanced CpG-stimulated iNOS expression. Further, we examined the macrophages phenotype switch based on characteristic expression profiles of surface markers by flow cytometry. As detected by flow cytometry, Figure 4C and 4D showed a dramatic increase in CD86 expression (a M1 marker) and very slight increases in CD206 expression (a M2 marker) with CpG stimulation. In accordance with previous results, PI3Kγ knockdown enhanced CpG-stimulated CD86 expression and reduced CD206 expression. These results demonstrated PI3Kγ inhibition effectively reprogramme TAMs toward M1 phenotype polarization and enhanced CpG ODNs activation function for the NF-kB signaling pathway in macrophages.

Antitumor effects of CpG-siRNA-tFNA

In the current study, we chose 4T1 breast cells as the typical tumorous cells to analyze anti-tumor activity of CpG-siRNA-tFNA treated macrophages. As showed in Figure 5A, RAW264.7 cells were cocultured with 4T1 cells in the Transwell system. CpG-stimulated macrophages revealed obvious anti-proliferative effects on 4T1 cells. More importantly, CpG-siRNA-tFNA treated macrophages showed higher anti-proliferative efficacy with PI3Kγ knockdown. Moreover, cellular viability of 4T1 cells declined rapidly with macrophages supernate concentration increasing (Figure 5B). Taken together, PI3Kγ inhibition further stimulated higher amounts of immune cytokines secretion in macrophages, which strongly inhibited the proliferation of 4T1 cells.

In this investigation, activity of caspase-3 also determined with the caspase-3 activity kit. In accordance with previous results, the activity of caspase-3 was significantly increased in the 4T1 cells incubated with macrophages together with CpG-tFNA or CpG-siRNA-tFNA (Figure 5C).

To further quantify apoptosis of tumor cells, we used flow cytometry to analyze the macrophages-mediated apoptosis after incubation with CpG-siRNA-tFNA for 24h. Resules showed that the apoptotic cell percentage obviously increased in CpG-tFNA and CpG-siRNA-tFNA groups compared with control group (Figure 5D and 5E). Clearly, these resules prove CpG-siRNA-tFNA treated macrophages effectively inhibit tumor cells proliferation and promote tumor cells apoptosis, which exhibit strong immunostimulatory and antitumor activity.

Conclusions

In summary, the study fabricated an efficient siRNAs and CpG ODNs delivery system (CpG-siRNA-tFNA) based on nucleic acid stepwise self-assembled with controllable loading density and high delivery efficiency. Moreover, the CpG-siRNA-tFNA effectively reprogramme TAMs toward M1 phenotype polarization with CpG ODNs immunostimulation and PI3Kγ expression downregulation. Furthermore, CpG-siRNA-tFNA induce macrophages dramatically upregulating proinflammatory cytokines together with the activated NF-κB signal pathways, which triggers apparent antitumor immune responses for the effective inhibition of tumor cells proliferation. Altogether, the results provide a rational basis for further development of the CpG-siRNA approach to targe TAMs for clinical applications.

Materials And Methods

Materials

All DNA oligonucleotide sequences were synthesized and purified by Sangon Biotechnology Co., Ltd. (Shanghai, China). PI3Kγ siRNA were designed and synthesized by GenePharma Co., Ltd. (Shanghai, China). All oligonucleotide sequences were showed in Table S1. Antibodies against PI3Kγ was purchased from Santa Cruz Biotechnology, Inc. (CA, USA). Antibodies for iNOS, Arg-1, NF-κB p65 and phospho-NF-κB p65 (Ser536) were obtained from Cell Signaling Technology (Danvers, USA). Antibodies against GAPDH and β-tubulin were purchased from Bioworld Technology Co., Ltd. (Nanjing, China). The anti-CD16/32,

anti-CD86 and anti-CD206 were obtained from BioLegend (San Diego, CA, USA). The horseradish peroxidase (HRP)-conjugated anti-rabbit IgG secondary antibodies were purchased from Beyotime Biotechnology Co., Ltd. (Shanghai, China). All ELISA kits were obtained from Bopei Biotechnology Co., Ltd. (Chongqing, China). Total RNA extraction kit was obtained from Promega (Madison, USA). The caspase-3 activity kit was purchased Beyotime Biotechnology Co., Ltd. (Shanghai, China). A PrimeScript™ RT reagent kit and a SYBR® Premix Ex Taq™ reagent kit were purchased from TaKaRa Biotechnology Co., Ltd. (Dalian, China). All ssDNAs were dissolved in sterile water and stored at -20°C. PI3Kγ siRNA were dissolved in DEPC water (Sangon, Shanghai, China).

Cell culture

The mouse breast cancer cell lines 4T1 and mouse macrophage cell line RAW264.7 were obtained from the American Type Culture Collection (ATCC; Rockville, MD, USA) and cultured in RPMI 1640 medium (Gibco, Grand Island, NY, USA) supplemented with 10% fetal bovine serum (Gibco, Grand Island, NY, USA) and 1% penicillin/streptomycin. All cell lines were incubated in an atmosphere of 5% CO_2 at 37°C according to ATCC guidelines.

Preparation of tFNA, CpG-tFNA and CpG-RNAi-tFNA

DNA self-assembly structures were prepared as reported previously. For tFNA, six different ssDNAs mixtures of component oligonucleotides (S1, S2, S3, S4, S5 and S6) were combined in TM buffer (10 mM Tris, 5 mM $MgCl_2$), heated to 95°C for 2 minutes, then rapidly cooled to 4°C in a T100^{TM} Thermal Cycler (Bio-Rad, Hercules, CA, USA). Each ssDNAs strand final concentration was 1mM. The CpG-tFNA and CpG-RNAi-tFNA were prepared in the same way.

Gel electrophoresis

Agarose gel electrophoresis was performed to confirm the successful assembly of tFNA, CpG-tFNA and CpG-RNAi-tFNA. The experiments were operated in 1 × TBE running buffer under the condition of 100 V voltage. After nucleic acid stain (gold view) disposed, the gel was visualized with imaging system (Bio-Rad, Hercules, CA, USA).

Stability analysis of tFNA

To test the nanostructures stability, tFNA and dsDNA were separately incubated with fetal bovine serum of equal volume at 37°C for different time periods (0, 3, 6, 12 and 24h). The mixtures were then subjected to 2% agarose gel.

Cellular Uptake

RAW264.7 cells were grown on glass cover slips in 24-well culture plates at a density of 5×10^5 cells/mL and incubated at 37°C for 24 h. They were then washed with sterile phosphate-buffered saline (PBS) and changed into fresh RPMI 1640 medium. Next, cells were separately incubated with fluorescently labeled

100 nM CpG and CpG-tFNA at 37℃. After culturing for 1 h, all cells were washed with pre-cold phosphate-buffered saline (PBS) three times and then fixed with 4% formaldehyde (Solarbio, Beijing, China) for 20 min at room temperature. And cells nuclei were treated with DAPI for 10 min. Finally, all confocal images were captured using a laser confocal microscope (Leica TCS SP8, Germany) and a fluorescence microscope (Nikon ECLIPSE Ti-s, Japan).

Cellular cytotoxicity assays

RAW264.7 cells were seeded in 96-well plate with 5×10^3 cells per well in 100 μL and cultured for cell adhesion. The medium was replaced by 100 μL fresh medium containing CpG-tFNA or CpG-RNAi-tFNA at different concentrations. The cells were further incubated for 48 h at 37°C. Then the medium was replaced by fresh culture medium and CCK-8 solution was added and incubated for 1 h. The absorbance at 450 nm was measured using a Model 680 microplate reader (Bio-Rad, Hercules, CA, USA).

Real-time PCR

Total RNA was harvested from RAW264.7 cells and reverse transcribed into cDNA. Relevant inflammatory cytokines gene (Il-6, Il-12, Tnfa) expression were determine according to the manufacturer's instruction. The sequences of primers were provided in Table S2. The reactions were performed in a volume of 10 μL using CFX96 Touch™ Real-Time PCR Detection System (Bio-Rad, Hercules, CA, USA).

ELISA assay

RAW264.7 cells were seeded in a 6-well plate and cultured for cell adhesion. Then, the medium was replaced by 2 mL fresh medium containing different concentrations CpG-tFNA or CpG-RNAi-tFNA for 24h. The supernatants were collected and the levels of cytokines were determined by an ELISA assay as the manufacturer's protocol.

Western blotting

Whole protein from RAW264.7 cells were harvested with RIPA buffer containing proteinase and phosphatase inhibitor cocktail. The protein concentration was measured by BCA assay. Protein samples were separated on SDS-polyacrylamide gels and transferred onto polyvinylidene difluoride (PVDF) membranes. The membranes were blocked with 5% non-fat dry milk in Tris-buffered saline with 0.05% Tween-20 (TBST) for 1 h followed by incubation at 4℃ overnight with the primary antibodies. HRP anti-rabbit IgG were used as the secondary antibodies. The signals were analyzed using an enhanced chemiluminescence detection system (Bio-Rad, Hercules, CA, USA).

Transwell assays

RAW264.7 cells and 4T1 cells were co-culture using the Transwell system (Millipore, Bedford, MA, USA) with 3 μm pore-size. Then CpG-tFNA and CpG-RNAi-tFNA were added to the upper chamber. After incubation for 48 h, the cell viability of 4T1 cells in the lower chambers was determined by a CCK-8 assay.

Caspase-3 activity assay

A transwell system (3μm-pore polycarbonate filter membrane) was performed to explore the antitumor effect of CpG-RNAi-tFNA. RAW264.7 cells and 4T1 cells were respectively added to the upper and lower chambers and cultured in RPMI 1640 medium containing 10% FBS for 24h. Then CpG-tFNA and CpG-RNAi-tFNA were added to the upper chamber. After incubation for 24h, the 4T1 cells were collected and the activity of caspase-3 was determined by the caspase-3 activity kit.

Apoptosis assay

4T1 cells were harvested with EDTA-free trypsin and washed with cold PBS for three times. Subsequently, the cells were resuspended in 500 μL PBS and stained with 5 μL Annexin V-fluorescein isothiocyanate (FITC) and 5 μL propidium iodide (PI) for 15 min in the dark at room temperature. Finally, the apoptosis of 4T1 cells were evaluated by FACScan flow cytometer (BD Biosciences).

Flow cytometry

Briefly, RAW264.7 cells were treated with CpG-siRNA-tFNA for 24h. Then, the cells were resuspended in 500 μL PBS and blocked with anti-CD16/32 for 10min at 4 °C. After washed with cold PBS, the cells were incubated with anti-CD86 and anti-CD206 for 30 min in darkness. Finally, the expression of CD86 and CD206 were evaluated by flow cytometry.

Statistical analysis

Student’s t-test or one-way analysis of variance (ANOVA) was used to assess the differences between treated and control groups. with GraphPad Prism 8. All quantitative results are presented as mean ± SD (standard deviation) with at least three independent repetitive experiments.

Abbreviations

TAMs: tumor-associated macrophages; TME: tumor microenvironment; CpG ODNs: cytosine-guanosine oligodeoxynucleotides; siRNA: small interfering RNA; ASO: antisense oligodeoxynucleotide; FNA: framework nucleic acid; tFNA: tetrahedral framework nucleic acid; TLR9: toll-like receptor 9; TLRs: toll-like receptors; PBS: phosphate-buffered saline; PVDF: polyvinylidene difluoride.

Declarations

Supplementary Material

Supplementary Material contains results, and figures. This content is available free of charge via the Internet.

Acknowledgements

This work was supported by the National Natural Science Foundation of China (No. 81772844 and No. 81873980) and Chongqing Medical University Graduate Talent Training Program (No. 172020220200033).

Authors' contributions

Husun Qian: cell experiments, drafting the manuscript, data acquisition, data analysis and manuscript revision. Yixin Fu, Minkang Guo and Wu Yang: material and technological support, data arrangement and analysis. Dian Zhang, Ting Zhou, Wenli Fang, Mengli Yao, He Shi and Chengsen, Chai: study concept, and supervision; Wei Cheng, Shijia Ding and Tingmei Chen: manuscript revision, study concept, design, supervision, and funding. All authors read and approved the fnal manuscript.

Availability of data and materials

The datasets used or analyzed during the current study are available from the corresponding author upon reasonable request.

Consent for publication

All authors agree to be published.

Competing Interests

The authors have declared that no competing interest exists.

References

1. Qian B-Z, Pollard JW. Macrophage diversity enhances tumor progression and metastasis. Cell. 2010; 141: 39-51.
2. Cassetta L, Pollard JW. Tumor-associated macrophages. Curr Biol. 2020; 30: R246-R8.
3. Chen Y, Song Y, Du W, Gong L, Chang H, Zou Z. Tumor-associated macrophages: an accomplice in solid tumor progression. J Biomed Sci. 2019; 26: 1-13.
4. Siveen K, Kuttan G. Role of macrophages in tumour progression. Immunol Lett. 2009; 123: 97-102.
5. Martinez FO, Sica A, Mantovani A, Locati M. Macrophage activation and polarization. Front Biosci. 2008; 13: 453-61.
6. Mantovani A, Sica A. Macrophages, innate immunity and cancer: balance, tolerance, and diversity. Curr Opin Immunol. 2010; 22: 231-7.
7. Liu Y-C, Zou X-B, Chai Y-F, Yao Y-M. Macrophage polarization in inflammatory diseases. Int J Biol Sci. 2014; 10: 520.
8. Orecchioni M, Ghosheh Y, Pramod AB, Ley K. Macrophage polarization: different gene signatures in M1 (LPS+) vs. classically and M2 (LPS–) vs. alternatively activated macrophages. Frontiers in immunology. 2019; 10: 1084.

9. Shu Y, Cheng P. Targeting tumor-associated macrophages for cancer immunotherapy. Biochimica et Biophysica Acta (BBA)-Reviews on Cancer. 2020: 188434.
10. Park JE, Dutta B, Tse SW, Gupta N, Tan CF, Low JK, et al. Hypoxia-induced tumor exosomes promote M2-like macrophage polarization of infiltrating myeloid cells and microRNA-mediated metabolic shift. Oncogene. 2019; 38: 5158-73.
11. Jing X, Yang F, Shao C, Wei K, Xie M, Shen H, et al. Role of hypoxia in cancer therapy by regulating the tumor microenvironment. Mol Cancer. 2019; 18: 157.
12. He Y, Cong C, He Y, Hao Z, Li C, Wang S, et al. Tumor hypoxia relief overcomes multidrug resistance and immune inhibition for self-enhanced photodynamic therapy. Chemical Engineering Journal. 2019; 375: 122079.
13. Heusinkveld M, van der Burg SH. Identification and manipulation of tumor associated macrophages in human cancers. J Transl Med. 2011; 9: 216.
14. Lissbrant IF, Stattin P, Wikstrom P, Damber J, Egevad L, Bergh A. Tumor associated macrophages in human prostate cancer: relation to clinicopathological variables and survival. Int J Oncol. 2000; 17: 445-96.
15. Zhang BC, Gao J, Wang J, Rao ZG, Wang BC, Gao JF. Tumor-associated macrophages infiltration is associated with peritumoral lymphangiogenesis and poor prognosis in lung adenocarcinoma. Med Oncol. 2011; 28: 1447-52.
16. Xu X, Gong X, Wang Y, Li J, Wang H, Wang J, et al. Reprogramming Tumor Associated Macrophages toward M1 Phenotypes with Nanomedicine for Anticancer Immunotherapy. Advanced Therapeutics. 2020; 3: 1900181.
17. Zang X, Zhang X, Zhao X, Hu H, Qiao M, Deng Y, et al. Targeted delivery of miRNA 155 to tumor associated macrophages for tumor immunotherapy. Mol Pharm. 2019; 16: 1714-22.
18. Merlano M, Abbona A, Denaro N, Garrone O. Knowing the tumour microenvironment to optimise immunotherapy. Acta Otorhinolaryngol Ital. 2019; 39: 2.
19. Nie W, Wu G, Zhang J, Huang LL, Ding J, Jiang A, et al. Responsive exosome nano-bioconjugates for synergistic cancer therapy. Angewandte Chemie. 2020; 132: 2034-8.
20. Yu M, Duan X, Cai Y, Zhang F, Jiang S, Han S, et al. Multifunctional nanoregulator reshapes immune microenvironment and enhances immune memory for tumor immunotherapy. Advanced Science. 2019; 6: 1900037.
21. Cai H, Shukla S, Steinmetz NF. The Antitumor Efficacy of CpG Oligonucleotides is Improved by Encapsulation in Plant Virus-Like Particles. Advanced Functional Materials. 2020; 30: 1908743.
22. Reynolds A, Leake D, Boese Q, Scaringe S, Marshall WS, Khvorova A. Rational siRNA design for RNA interference. Nat Biotechnol. 2004; 22: 326-30.
23. Hu B, Zhong L, Weng Y, Peng L, Huang Y, Zhao Y, et al. Therapeutic siRNA: state of the art. Signal transduction and targeted therapy. 2020; 5: 1-25.

24. Xia H, Mao Q, Paulson HL, Davidson BL. siRNA-mediated gene silencing in vitro and in vivo. Nat Biotechnol. 2002; 20: 1006-10.
25. Gavrilov K, Saltzman WM. Therapeutic siRNA: principles, challenges, and strategies. The Yale journal of biology and medicine. 2012; 85: 187.
26. Wang T, Shigdar S, Al Shamaileh H, Gantier MP, Yin W, Xiang D, et al. Challenges and opportunities for siRNA-based cancer treatment. Cancer letters. 2017; 387: 77-83.
27. Ge Z, Gu H, Li Q, Fan C. Concept and development of framework nucleic acids. Journal of the American Chemical Society. 2018; 140: 17808-19.
28. Zhang T, Cui W, Tian T, Shi S, Lin Y. Progress in Biomedical Applications of Tetrahedral Framework Nucleic Acid-Based Functional Systems. ACS Applied Materials & Interfaces. 2020; 12: 47115-26.
29. Xue H, Ding F, Zhang J, Guo Y, Gao X, Feng J, et al. DNA tetrahedron-based nanogels for siRNA delivery and gene silencing. Chem Commun (Camb). 2019; 55: 4222-5.
30. Liu J, Song L, Liu S, Zhao S, Jiang Q, Ding B. A Tailored DNA Nanoplatform for Synergistic RNAi-/Chemotherapy of Multidrug-Resistant Tumors. Angew Chem Int Ed Engl. 2018; 57: 15486-90.
31. Ruan W, Zheng M, An Y, Liu Y, Lovejoy DB, Hao M, et al. DNA nanoclew templated spherical nucleic acids for siRNA delivery. Chem Commun (Camb). 2018; 54: 3609-12.
32. Bujold KE, Hsu JCC, Sleiman HF. Optimized DNA "Nanosuitcases" for Encapsulation and Conditional Release of siRNA. J Am Chem Soc. 2016; 138: 14030-8.
33. Bode C, Zhao G, Steinhagen F, Kinjo T, Klinman DM. CpG DNA as a vaccine adjuvant. Expert review of vaccines. 2011; 10: 499-511.
34. Vollmer J. CpG motifs to modulate innate and adaptive immune responses. Int Rev Immunol. 2006; 25: 125-34.
35. Krieg AM. Toll-like receptor 9 (TLR9) agonists in the treatment of cancer. Oncogene. 2008; 27: 161-7.
36. Kaneda MM, Messer KS, Ralainirina N, Li H, Leem CJ, Gorjestani S, et al. PI3Kγ is a molecular switch that controls immune suppression. Nature. 2016; 539: 437-42.
37. De Henau O, Rausch M, Winkler D, Campesato LF, Liu C, Cymerman DH, et al. Overcoming resistance to checkpoint blockade therapy by targeting PI3Kγ in myeloid cells. Nature. 2016; 539: 443-7.
38. Lee YS, Song SJ, Hong HK, Oh BY, Lee WY, Cho YB. The FBW7-MCL-1 axis is key in M1 and M2 macrophage-related colon cancer cell progression: validating the immunotherapeutic value of targeting PI3Kγ. Exp Mol Med. 2020: 1-17.
39. Luo L, Wall AA, Tong SJ, Hung Y, Xiao Z, Tarique AA, et al. TLR crosstalk activates LRP1 to recruit Rab8a and PI3Kγ for suppression of inflammatory responses. Cell Rep. 2018; 24: 3033-44.
40. Wall AA, Luo L, Hung Y, Tong SJ, Condon ND, Blumenthal A, et al. Rab8a recruited PI3Kγ regulates signaling and cytokine outputs from endosomal Toll-like receptors. J Biol Chem. 2017: jbc. M116. 766337.
41. Xie N, Huang J, Yang X, Yang Y, Quan K, Wang H, et al. A DNA tetrahedron-based molecular beacon for tumor-related mRNA detection in living cells. Chem Commun. 2016; 52: 2346-9.

Figures

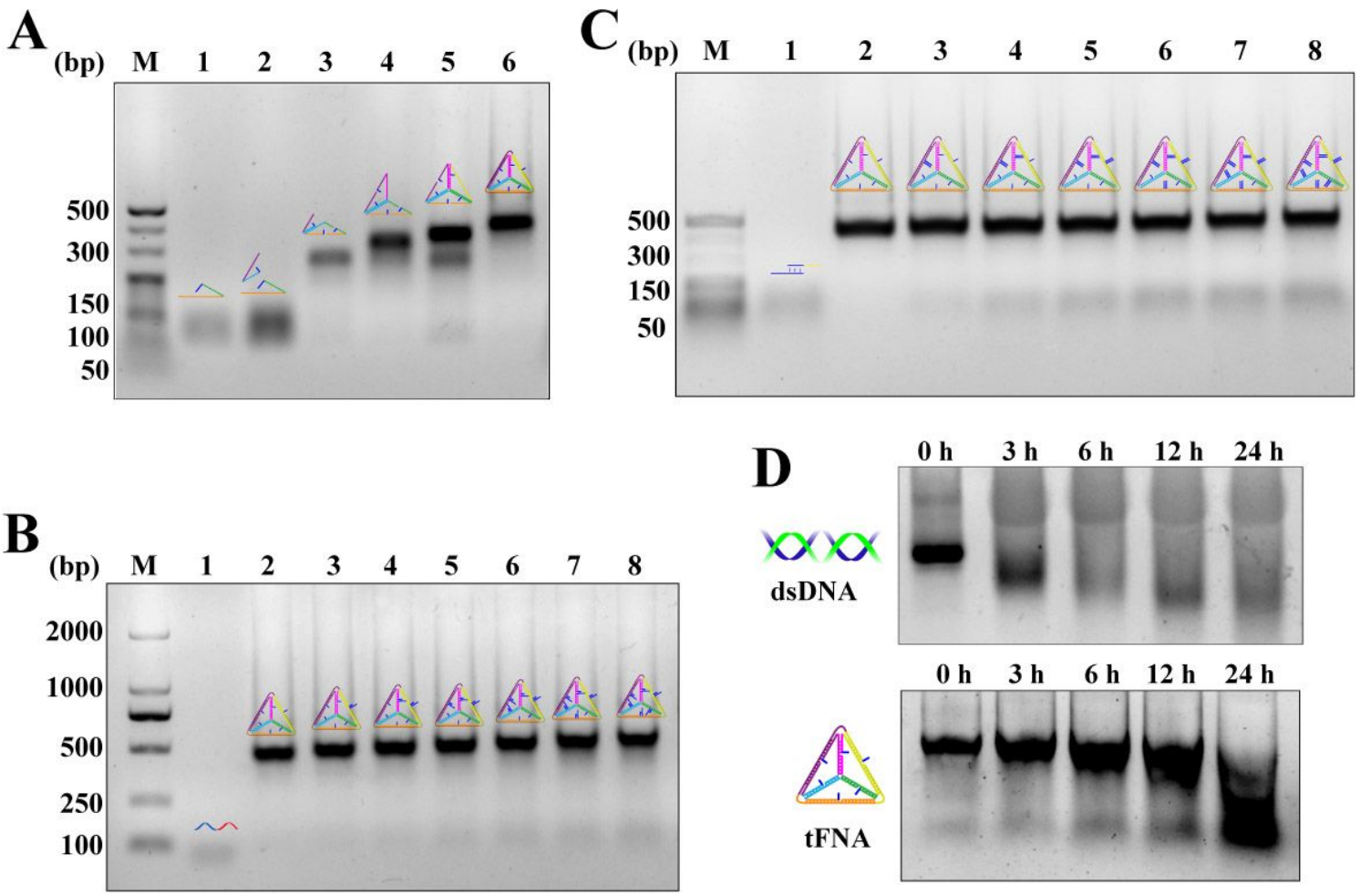

Figure 1

(A) Agarose gel electrophoresis analysis to confirm self-assembly of the tFNA (Lane 1, S1. Lane 2, S1 + S2. Lane 3, S1 + S2 + S3. Lane 4, S1 + S2 + S3 + S4. Lane 5, S1 + S2 + S3 + S4 + S5. Lane 6, S1 + S2 + S3 + S4 + S5 + S6, tFNA). (B) Agarose gel electrophoresis analysis to confirm the hybridization of CpG ODNs to the tFNA (Lane 1, CpG-overhang. Lane 2, tFNA. Lane 3, tFNA with 1 CpG. Lane 4, tFNA with 2 CpG. Lane 5, tFNA with 3 CpG. Lane 6, tFNA with 4 CpG. Lane 7, tFNA with 5 CpG. Lane 8, tFNA with 6 CpG). (C) Agarose gel electrophoresis analysis to confirm the hybridization of siRNA to the tFNA (Lane 1, CpG-overhang. Lane 2, tFNA. Lane 3, tFNA with 1 siRNA. Lane 4, tFNA with 2 siRNA. Lane 5, tFNA with 3 siRNA. Lane 6, tFNA with 4 siRNA. Lane 7, tFNA with 5 siRNA. Lane 8, tFNA with 6 siRNA). (D) Electrophoretic analysis of the stability of tFNA.

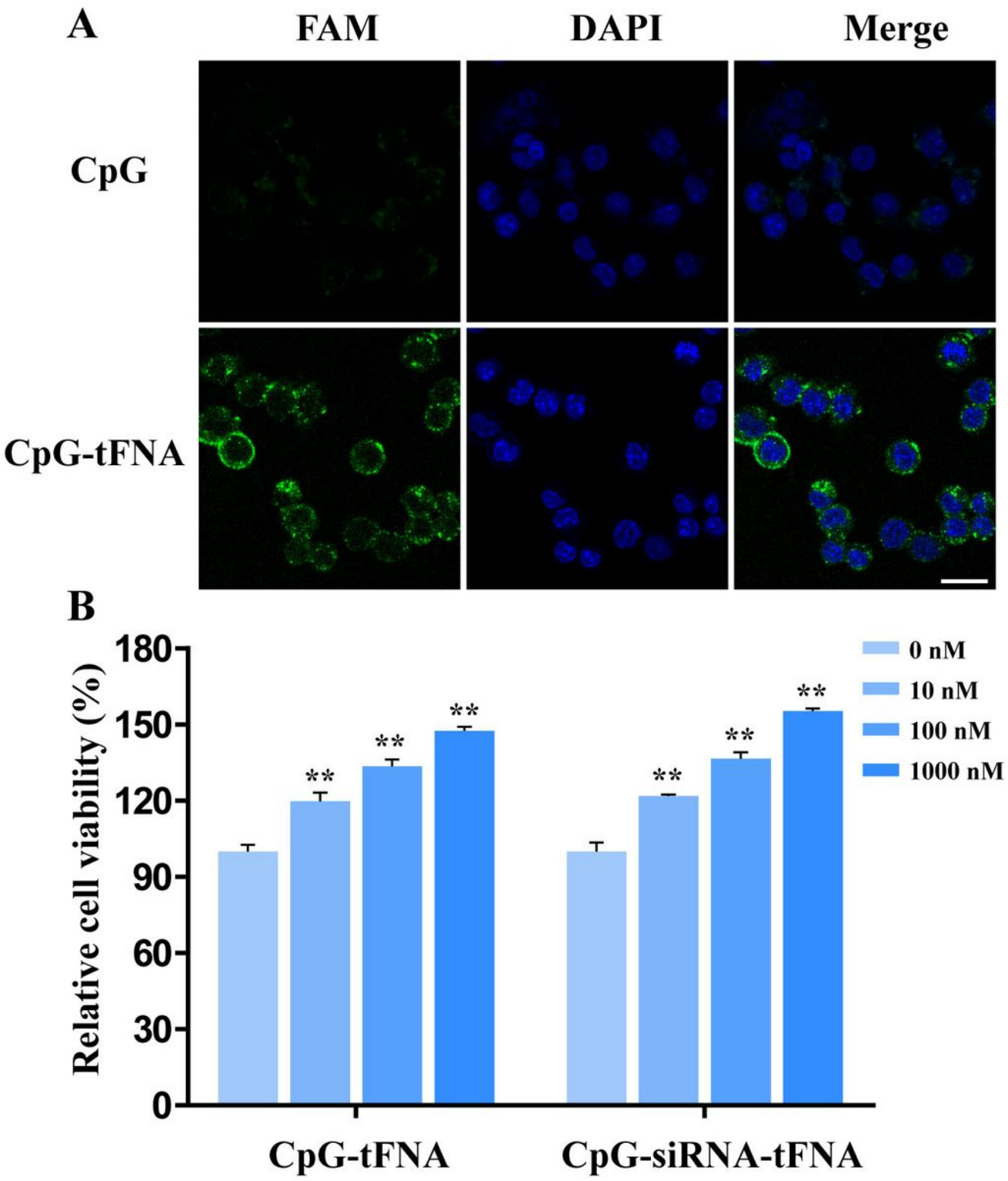

Figure 2

(A) Confocal laser scanning microscopy images analysis the difference of cellular uptake between CpG and CpG-tFNA. (B) Cell viability assay (CCK-8 assay) of RAW264.7 cells after treatment with different concentration CpG-tFNA and CpG-siRNA-tFNA for 24 h. The error bars are standard deviations of three repetitive measurements.

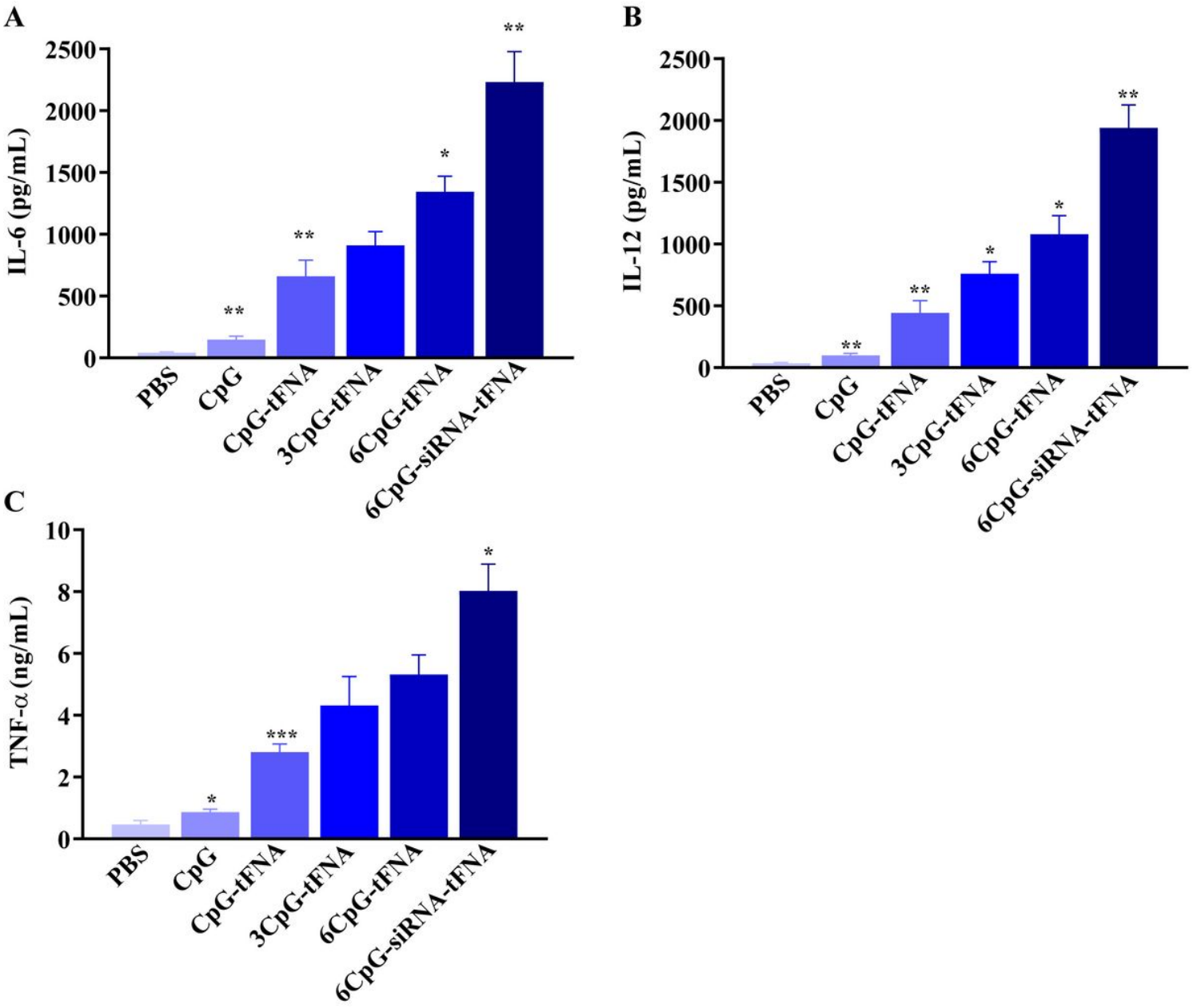

Figure 3

Proinflammatory cytokines (TNF-α, IL-6, and IL-12) secretions of RAW264.7 cells after being treated by different immunomodulatory agents for 24 h. The error bars are standard deviations of three repetitive measurements.

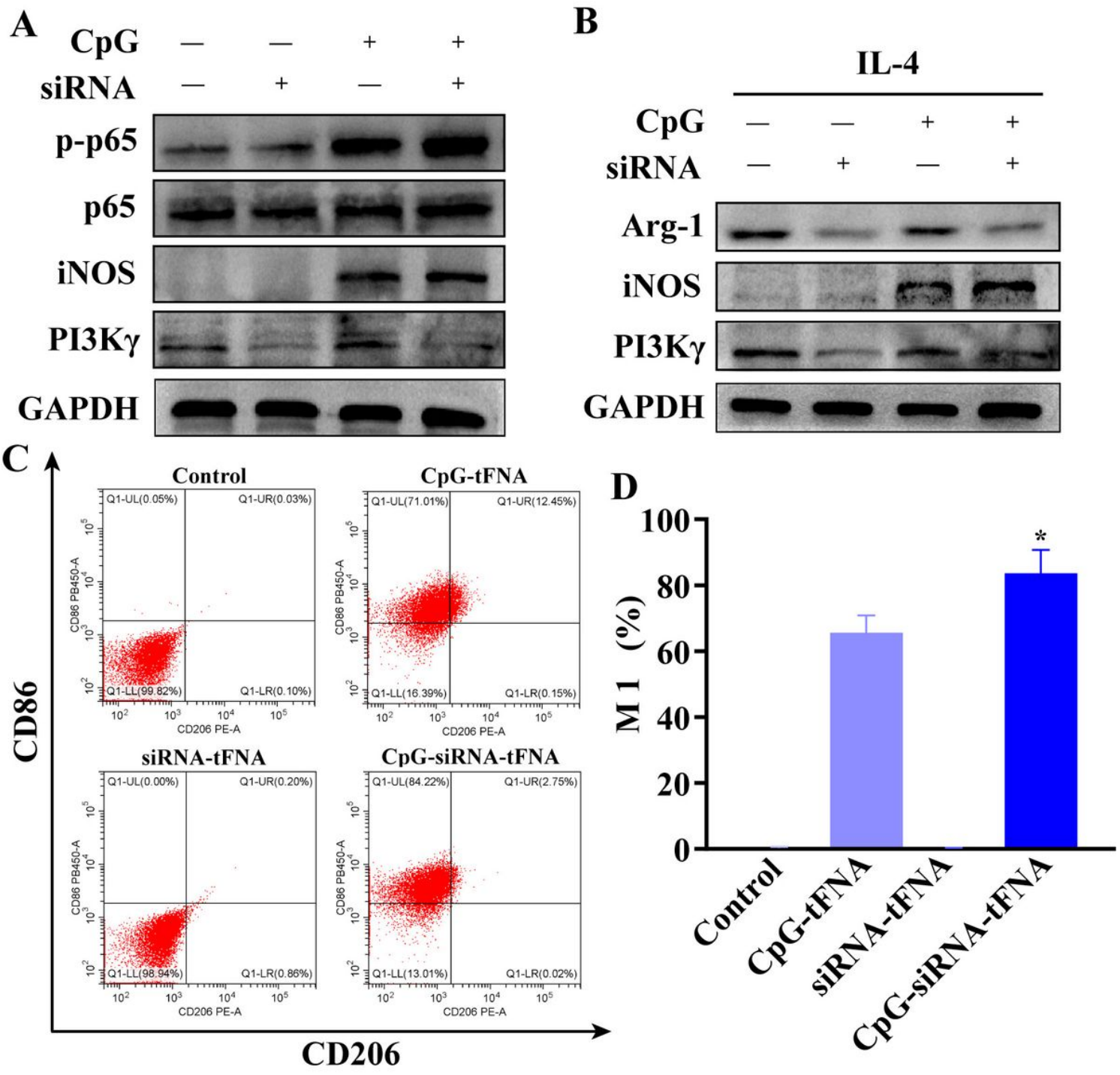

Figure 4

(A, B) Western blot analysis proteins expression involved in NF-κB signal pathways and macrophages markers in RAW264.7 cells. (C) Flow cytometry analysis the expression of CD86 and CD206 in RAW264.7 cells after treatment with different immunomodulatory agents for 24 h. (D) Statistical analysis of data. The error bars are standard deviations of three repetitive measurements.

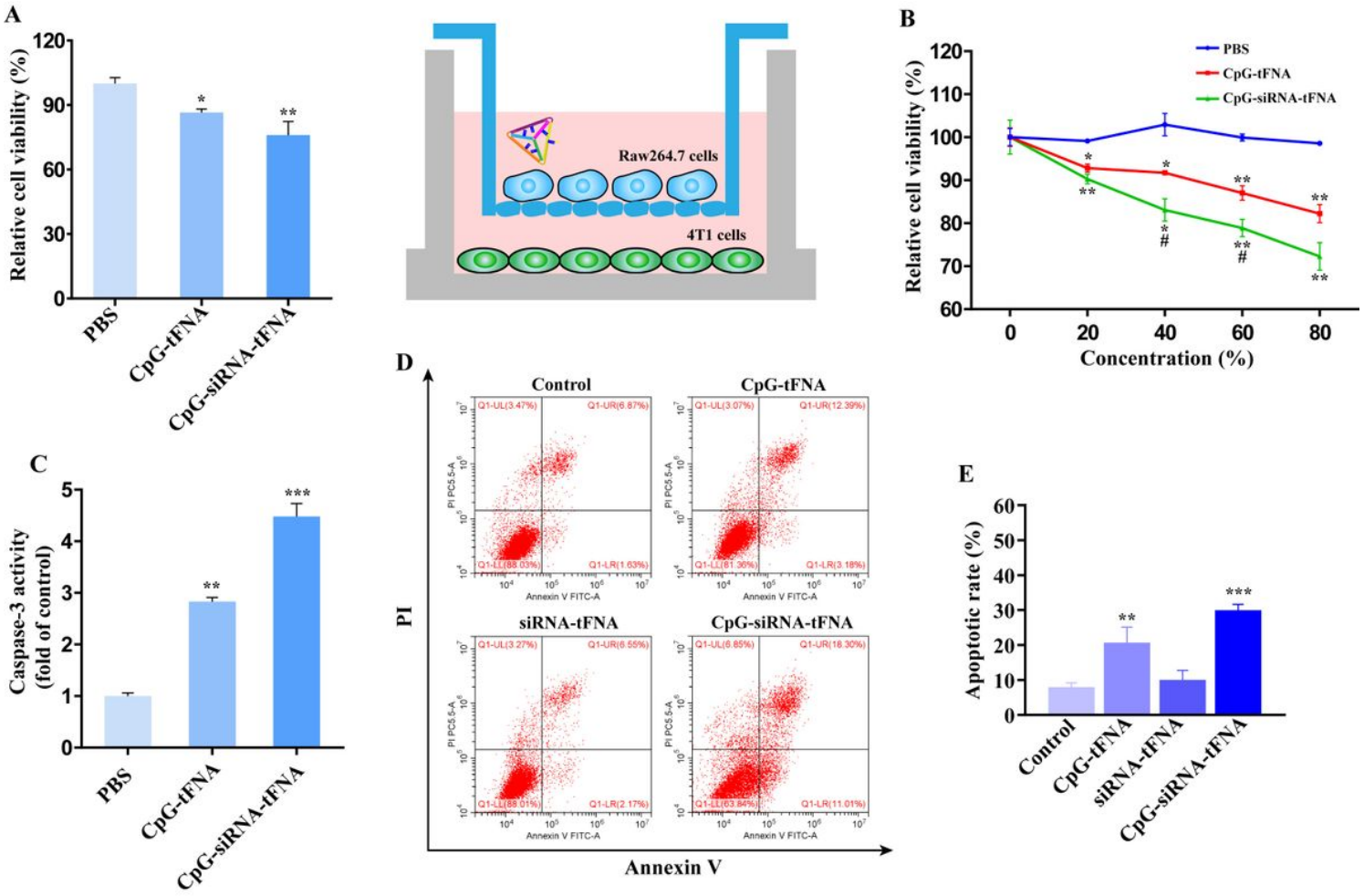

Figure 5

(A) RAW264.7 cells were cocultured with 4T1 cells in the Transwell system and the cell viability was assessed by the CCK-8 assay. (B) 4T1 cells were incubated with different concentration macrophages supernate and cell viability was assessed by the CCK-8 assay. (C) The activity of 4T1 cells caspase-3 was determined in vitro. (D) Cell apoptosis was detected by flow cytometry at 24 h. (E) Statistical analysis of data. The error bars are standard deviations of three repetitive measurements.

Supplementary Files

This is a list of supplementary files associated with this preprint. Click to download.

- SupplementaryMaterial.docx
- GraphicalAbstract.tif
- Scheme1.tif